R26

A Close-in LiDAR for Diffusive Media based on a 32 × 32 CMOS SPAD Image Sensor

Scott Lindner[1,2], Chao Zhang[3], Alexander Kalyanov[2], Martin Wolf[2], Claudio Bruschini[1], Edoardo Charbon[1]

[1]EPFL, Neuchâtel, Switzerland
Address: Rue de la Maladière 71b , 2002 Neuchâtel, Switzerland
Email: scott.lindner@epfl.ch
[2]University of Zurich, Zurich, Switzerland
[3]TUDelft, Delft, The Netherlands

Introduction

The ability of light detection and ranging (LiDAR) systems to provide depth information of a scene has already sparked development and application in a wide range of areas, e.g. self-driving vehicles, video game systems, industrial automation, etc. These developments have focused on applications where the surface of objects under study provides a reflection, and the non-reflected light is absorbed. This eases the depth reconstruction since received light can be assumed to have reflected from the object's surface. There are, however, applications where this is not the case, for example, in robotic-assisted surgery [1], where surgical instruments are inserted into the patient through small incisions. Here, a LiDAR could provide the surgeon with an accurate spatial map of the surgical environment, in particular the position of instruments in relation to the tissue. Additionally, a map of the tissue boundary would be important for applications which aim to provide information from within the medium, e.g. fluorescence lifetime imaging [2]. Such applications are enabled by the presence of an 'optical window' between 600 and 900 nm, in which light incident onto the surface can penetrate tissue for several centimeters. For the non-absorbed light, the scattering nature of tissue results in the diffusion of light into the tissue surface. This is demonstrated on a silicone phantom shown in Fig. 1. This presents a major challenge for LiDAR at these wavelengths, since light which returns to the sensor is not solely from a reflection from the surface. An alternative solution could be to operate with light at a shorter wavelength, e.g. green, however, this would require an additional laser for applications which seek to image beneath the surface whilst also being visible to the operator and any other instruments.

In this work, we present a close-in LiDAR based on a 32 × 32 time-resolved CMOS SPAD image sensor [3], shown in Fig 2. The time-resolved histograms provide a means by which the diffuse photons can be discriminated from those immediately reflected, as they result in a later time-of-arrival, shown in Fig. 3.

System Ranging Performance

To demonstrate system accuracy for demanding applications, we employ the system as a single-point telemeter with no optics attached to the camera, as depicted in Fig. 4. A square piece of white paper is attached to a plastic stand, which is mounted on a precision motorized linear stage (LTM 80, Owis GmbH) at a distance of 56 cm from the camera. Pulsed light is provided by a super continuum laser (SuperK Extreme, Nkt Photonics) with acousto-optic tuneable filter (SuperK Select, NkT Photonics) at a wavelength of 900 nm. The paper is illuminated with a single point provided by a collimator and adjustable pin-hole to produce a beam-spot of approximately 1 mm diameter with average illumination power of 98.4 µW. The collimator is placed next to the camera whilst the linear stage moves the position of the paper over a distance of 70 mm in steps of 1 mm, pausing after each step to acquire data. Each acquisition comprises around 25 kphotons for the entire array and requires 50 ms. Additionally, due to the readout mode, only 25% of detected photons are read out. Thus, with a full speed readout the acquisition time would equal 12.5 ms. Acquired data is corrected in post-processing to account for TDC least-significant bit (LSB) mismatch and to cancel buffer delays between the pixels and the TDCs. To obtain sufficient performance statistics, the linear-stage traversed the 70 mm distance 25 times. Distance is determined using the first-moment, m_1, of the timing histogram. Non-linearity in comparison to the ground truth shows a non-linearity of +0.82/-0.62 mm over the entire range, Fig. 5. Precision is obtained by measuring the standard deviation of the 25 measurements at each distance, Fig. 6., showing a worst-case precision of 0.94 mm.

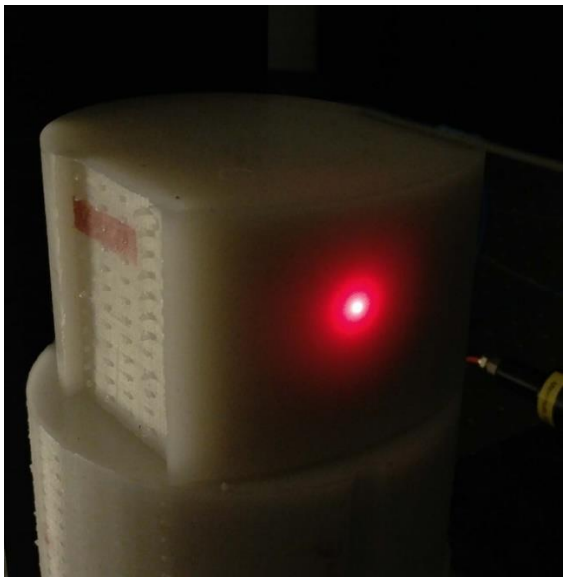

Fig. 1. Light diffusing into silicone phantom with absorption coefficient, μ_a = 0.0035 mm^{-1}, and reduced scattering coefficient, $\mu_{s'}$ = 0.6 mm^{-1}.

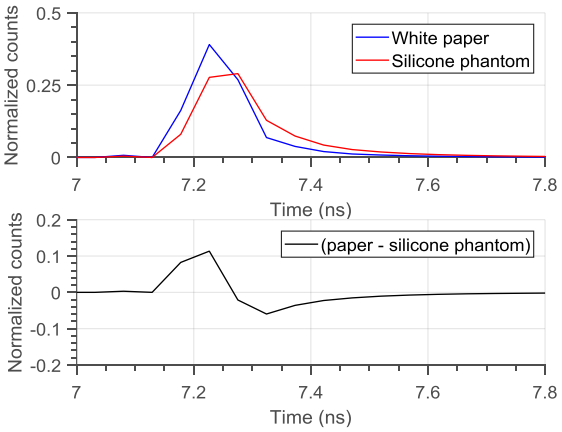

Fig. 3. Comparison of timing histogram between white paper and silicone phantom in same position, histograms (top) and difference (bottom).

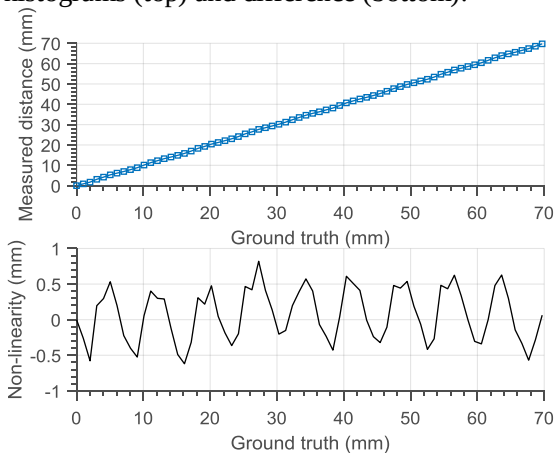

Fig. 5. Non-linearity of single-point telemetry with white paper target at 900 nm.

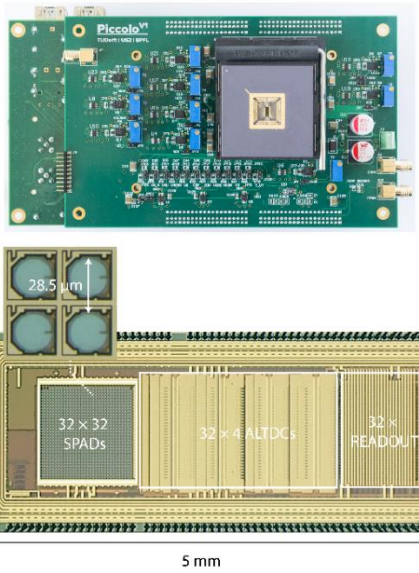

Fig. 2. Piccolo, 32 × 32 time-resolved CMOS SPAD image sensor PCB (top) and micrograph with pixel inset (bottom).

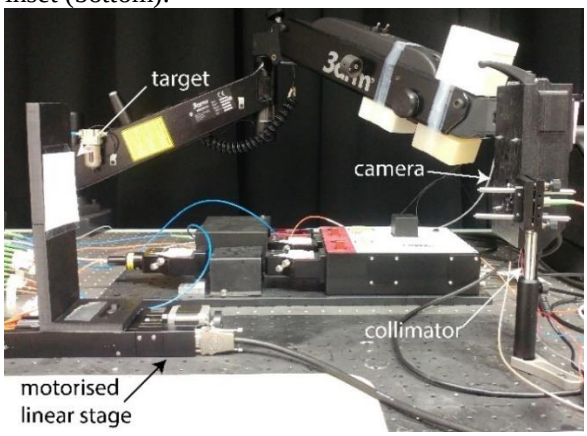

Fig. 4. Lab setup for single-point telemetry measurements.

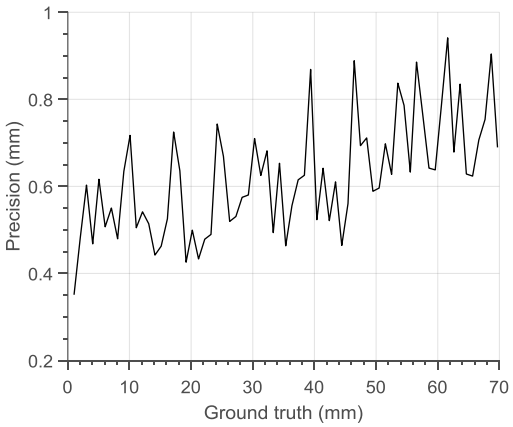

Fig. 6. Precision (σ) of single-point telemetry with white paper target at 900nm.

Normalized Gradient (ng) Method

To measure a time-of-flight distance with an accuracy better than the least-significant bit (LSB) of the sensor, i.e. 48.8 ps, the first moment, m_1, of the timing response is typically calculated [4]. This is unsuitable for diffuse media since a significant number of photons diffuse into the surface before being ejected, and detected. Since the arrival time of these photons carries information on the structure of the medium, diffuse light propagation within the medium biases the calculation of m_1, and thus the measurement of distance. We propose a method which calculates the distance based on the bins in the vicinity of the histogram peak. This reduces the influence of diffuse photons which appear later in the timing response. We define a parameter, the normalized gradient (ng), equal to $(y_{max} - y_{max-1})/y_{max}$, where y_{max} and y_{max-1} are the number of counts in the histogram peak and the preceding bin, respectively. This is shown graphically in Fig. 7. The ng is a monotonic function with a period of 1 LSB, as seen in Fig. 8. It is obtained through simulation by interpolating the timing response of a pixel, shifting it in small steps over 1 LSB and quantizing it at each step with the resolution of the TDC. With the ng calculated at every step, each ng is mapped to a time-shift. A distance can then be obtained by measuring the ng of the histogram, and summing the peak index with the time shift obtained by the ng. This is demonstrated by applying the method to the telemetry data of the previous section. Non-linearity and precision are shown in Figures 9 and 10, respectively, showing a non-linearity of +1.85/-1.86 mm and worst- case precision of 1.23 mm.

The ng algorithm is evaluated for the diffuse medium case by mounting a silicone phantom on the precision linear stage and illuminating it with a collimated beam spot (840 nm). A timing histogram is obtained for a single pixel focused on the beam spot in the cases where light is incident on the phantom and when the phantom is covered with white paper, Fig. 11. The distance is calculated for both cases with both ng and m_1. The results, Fig. 12., show that the measurement error between reflective (paper) and diffuse (silicone phantom) cases can be reduced from the range of 7.8 – 14 mm using m_1, to 3.1 – 5.9 mm with the ng approach. This demonstrates that the ng method is less biased by photons which diffuse into the phantom. Importantly, the simulation to obtain the ng function was performed using data from a reflective experiment. Thus, it is reasonable to assume that the results could be further improved by obtaining the ng function from the medium to be measured. From an applications perspective, this implies using either prior knowledge of the surface type or determining the surface type through analysis of the timing histogram.

Conclusions

We presented a SPAD based LiDAR for determining the boundaries of diffuse media. Measurements with a linear stage and a reflective target demonstrated that a high degree of ranging accuracy can be obtained. We proposed a ranging algorithm which computes the distance with a sub-LSB resolution using photons in the vicinity of the peak of the timing histogram. Comparison measurements on a silicone phantom demonstrate a greater resilience to the bias of photons diffusing into the medium than m_1. Future measurements involving surface type dependent computation of the ng function promise to further improve results.

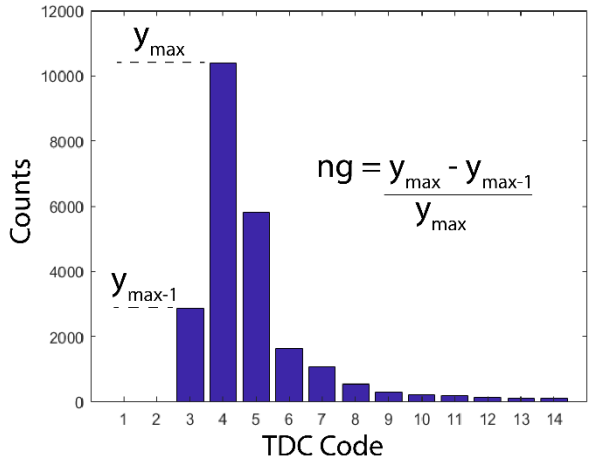

Fig. 7. Graphical depiction of normalized gradient calculation

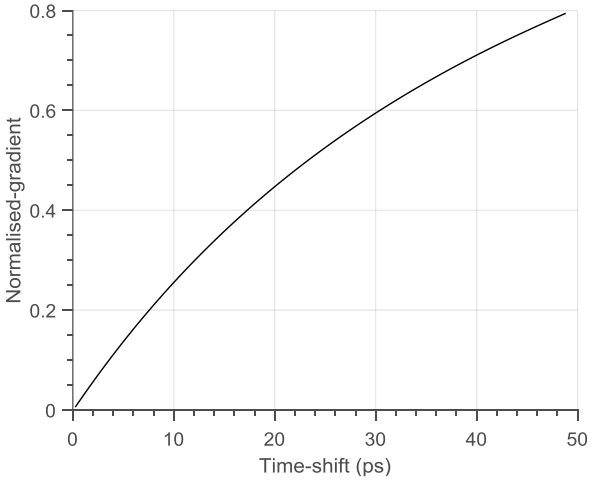

Fig. 8. Normalized gradient function for a typical pixel

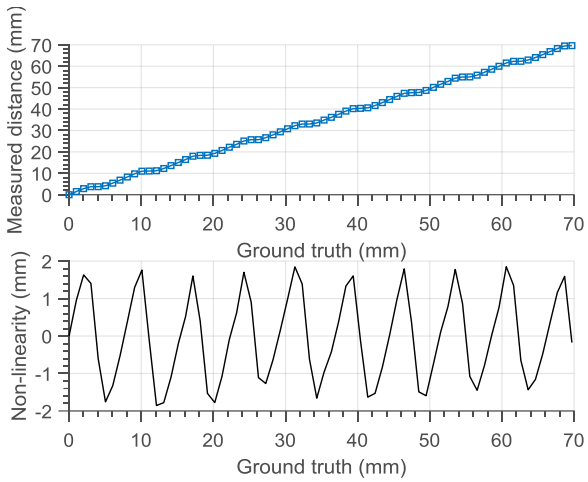

Fig. 9. Non-linearity of single-point telemetry using ng algorithm.

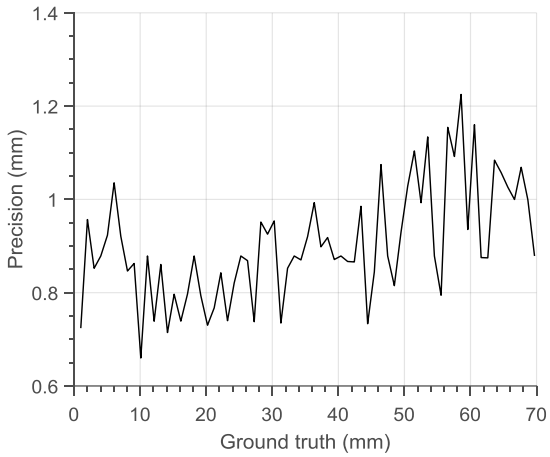

Fig. 10. Precision (σ) of single-point telemetry with white paper target using ng algorithm.

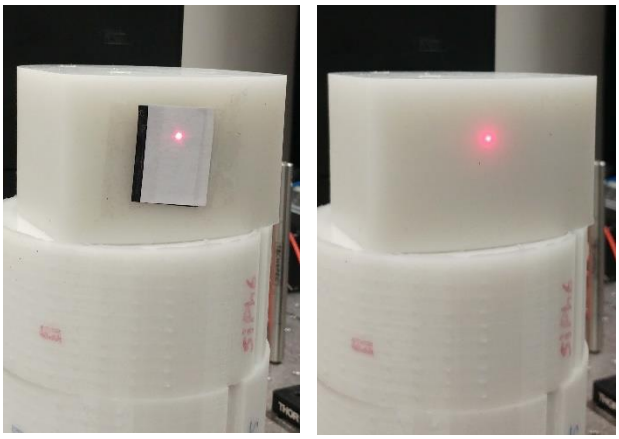

Fig. 11. Setup for comparison of m_1 and ng algorithms. Phantom is measured with point illumination with white paper at beam spot (left), and bare (right). Target is moved over 10 mm in 1mm steps.

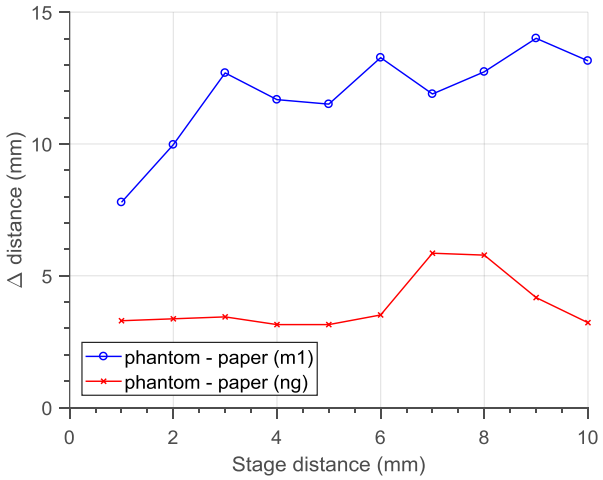

Fig. 12. Difference in distance calculation at 840 nm for a single pixel for m_1 and ng, between when phantom is bare and phantom is covered with paper.

Acknowledgements

The authors would like to acknowledge support from Intuitive Surgical Inc.

References

[1] M. Diana and J. Marescaux (2015), "Robotic surgery". British Journal of Surgery, 102: e15-e28.

[2] Klaus Suhling et al, "Fluorescence lifetime imaging (FLIM): Basic concepts and some recent developments". Medical Photonics, Volume 27, 2015.

[3] C. Zhang, S. Lindner, I.M. Antolovic, M. Wolf, E. Charbon, "A CMOS SPAD Imager with Collision Detection and 128 Dynamically Reallocating TDCs for Single-Photon Counting and 3D Time-of-Flight Imaging". *Sensors*, 2018, *18*, 4016.

[4] C. Niclass, C. Favi, T. Kluter, M. Gersbach and E. Charbon, "A 128 × 128 Single-Photon Image Sensor With Column-Level 10-Bit Time-to-Digital Converter Array," in *IEEE Journal of Solid-State Circuits*, vol. 43, no. 12, pp. 2977-2989, Dec. 2008.